A dynamical (e,2e) investigation of the structurally related cyclic ethers tetrahydrofuran, tetrahydropyran, and 1,4-dioxane

J. D. Builth-Williams, S. M. Bellm, L. Chiari, P. A. Thorn, D. B. Jones, H. Chaluvadi, D. H. Madison, C. G. Ning, B. Lohmann, G. B. da Silva, and M. J. Brunger

Citation: The Journal of Chemical Physics **139**, 034306 (2013); doi: 10.1063/1.4813237
View online: http://dx.doi.org/10.1063/1.4813237
View Table of Contents: http://scitation.aip.org/content/aip/journal/jcp/139/3?ver=pdfcov
Published by the AIP Publishing

A dynamical (e,2e) investigation of the structurally related cyclic ethers tetrahydrofuran, tetrahydropyran, and 1,4-dioxane

J. D. Builth-Williams,[1] S. M. Bellm,[1] L. Chiari,[1] P. A. Thorn,[1] D. B. Jones,[2,a)] H. Chaluvadi,[3] D. H. Madison,[3] C. G. Ning,[4] B. Lohmann,[5] G. B. da Silva,[1,6] and M. J. Brunger[1,7,a)]
[1]*ARC Centre of Excellence for Antimatter-Matter Studies, Flinders University, GPO Box 2100, Adelaide, South Australia 5001, Australia*
[2]*School of Chemical and Physical Sciences, Flinders University, GPO Box 2100, Adelaide, South Australia 5001, Australia*
[3]*Department of Physics, Missouri University of Science and Technology, Rolla, Missouri 65409, USA*
[4]*Department of Physics, State Key Laboratory of Low-Dimensional Quantum Physics, Tsinghua University, Beijing 100084, China*
[5]*University of the Sunshine Coast, Maroochydore DC, Queensland 4558, Australia*
[6]*Universidade Federal de Mato Grosso, Barra do Garças, Mato Grosso, Brazil*
[7]*Institute of Mathematical Sciences, University of Malaya, 50603 Kuala Lumpur, Malaysia*

(Received 3 May 2013; accepted 24 June 2013; published online 17 July 2013)

Triple differential cross section measurements for the electron-impact ionization of the highest occupied molecular orbitals of tetrahydropyran and 1,4-dioxane are presented. For each molecule, experimental measurements were performed using the (e,2e) technique in asymmetric coplanar kinematics with an incident electron energy of 250 eV and an ejected electron energy of 20 eV. With the scattered electrons being detected at -5°, the angular distributions of the ejected electrons in the binary and recoil regions were observed. These measurements are compared with calculations performed within the molecular 3-body distorted wave model. Here, reasonable agreement was observed between the theoretical model and the experimental measurements. These measurements are compared with results from a recent study on tetrahydrofuran [D. B. Jones, J. D. Builth-Williams, S. M. Bellm, L. Chiari, C. G. Ning, H. Chaluvadi, B. Lohmann, O. Ingolfsson, D. Madison, and M. J. Brunger, Chem. Phys. Lett. **572**, 32 (2013)] in order to evaluate the influence of structure on the dynamics of the ionization process across this series of cyclic ethers. © *2013 AIP Publishing LLC*. [http://dx.doi.org/10.1063/1.4813237]

I. INTRODUCTION

Electron-matter interactions play key roles in the processes relating to terrestrial and atmospheric phenomena and plasma processing.[1] Recently, positron- and electron-interactions in biological systems have attracted significant attention[2,3] owing to the large number of secondary electrons that are produced from a single ionizing particle.[4] Here, the low-energy secondary electrons can deposit energy through ro-vibrational or electronic excitations or induce damage to the system through ionization or dissociative electron attachment processes.[5] In particular, recent studies have revealed that low-energy electron interactions with DNA can induce single and double strand breakage.[6,7] This has created a pressing demand for electron-impact collision cross section data with biological analogues that can be used for simulating radiation-induced damage to biological media. Further, collision cross section data may also provide clues for understanding radiation-induced phenomena in larger macro-molecular environments.

The experimental difficulties in measuring collision cross sections for many biological species have, however, limited the availability of data. This is particularly true for solid targets, such as the DNA bases. As such, it is imperative that theoretical models be developed that can accurately simulate data for species for which no experimental data are currently available. In this respect, studies on electron-induced phenomena on a series of chemically similar compounds serve as a method for providing benchmark experimental cross section data that can test and assess the limitations of the theoretical models. Such studies represent an important step in understanding how the structure of a species can influence the electron scattering phenomena. In this vein, we have recently extended some of our earlier studies on individual biomolecules[8–14] to chemically similar compounds in an attempt to further understand the role of structure and kinematics on the dynamics of electron-impact ionization.[15]

Building on that work, we present a dynamical (e,2e) investigation to compare the electron-impact ionization process across a series of cyclic ethers: tetrahydrofuran (THF, C_4H_8O), tetrahydropyran (THP, $C_5H_{10}O$), and 1,4-dioxane ($C_4H_8O_2$). These species are shown schematically in Fig. 1. Note that previous measurements of total cross sections for electron[16,17] and positron scattering[18] from series of structurally related cyclic ethers have been useful in establishing trends in their scattering phenomena. Further, they have revealed the potential for constructing functional forms for

a)Authors to whom correspondence should be addressed. Electronic addresses: darryl.jones@flinders.edu.au and michael.brunger@flinders.edu.au.

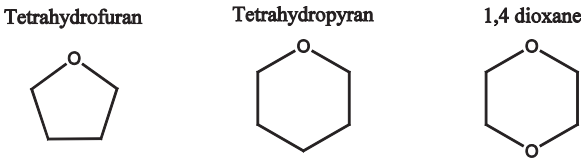

FIG. 1. The structure of the cyclic ethers: (a) tetrahydrofuran, (b) tetrahydropyran, and (c) 1,4-dioxane.

describing the total scattering cross section in both the electron and positron scattering cases. As such, a dynamical (e,2e) investigation of these cyclic ethers may provide key insights into the nature of ionization phenomena.

In this paper, we therefore supplement the existing data for electron-impact dynamical ionization of THF[12–15] with the first dynamical (e,2e) measurements for THP and 1,4-dioxane. Specifically, we present triple differential cross section (TDCS) measurements for the ionization of the highest occupied molecular orbital (HOMO) for each of these species. For these cyclic ethers, the HOMOs are expected to be dominated by the non-bonding out-of-plane lone-electron pair contributions from the oxygen atom(s). With qualitatively similar orbital structures for each target, the present results may thus be expected to provide detailed information into the influence that structure plays on the dynamics of the electron-impact ionization process. For our TDCS measurements, we select kinematical conditions that fall below the bound Bethe ridge condition. In our previous work on large biomolecules, these kinematical conditions exhibited the most sensitivity regarding the observed binary to recoil peak ratios.

The paper is organized as follows. In Sec. II, we present our experimental details and measurement techniques. This is followed by a discussion of the theoretical methods employed in Sec. III. We next provide a summary of the spectroscopy of the cyclic ethers, and how it impacts on their electron scattering phenomena. Our results are then presented and discussed in Sec. V. Following this, the conclusions drawn from this investigation are summarized.

II. EXPERIMENTAL METHOD

Triple differential cross sections for the electron-impact ionization of cyclic ethers have been measured under coplanar asymmetric kinematical conditions using a (e,2e) coincidence technique. These processes are described by

$$e_0^-(E_0, \boldsymbol{p}_0) + T \rightarrow T^+(\in_i, \boldsymbol{q}) + e_a^-(E_a, \boldsymbol{p}_a) + e_b^-(E_b, \boldsymbol{p}_b), \tag{1}$$

where the target, T, is either THP or 1,4-dioxane. In Eq. (1), E_j and $\boldsymbol{p}_j$ ($j = 0$, a, or b) are the energies and momenta of the incident, scattered, and ejected electrons, respectively. Here the conservation of energy during the collision determines the binding energy ($\in_i$) of the ionized orbital:

$$\in_i = E_0 - (E_a + E_b). \tag{2}$$

Likewise, the recoil momentum of the target ion is determined by the conservation of momentum:

$$\boldsymbol{q} = \boldsymbol{p}_0 - (\boldsymbol{p}_a + \boldsymbol{p}_b). \tag{3}$$

In the present experiments, the incident electron and ejected electron energies are fixed at $E_0 = 250$ eV and $E_b = 20$ eV, respectively. The scattered electron is detected at a fixed polar angle, $\theta_a = -5^\circ$, made with respect to the incident electron beam direction. The momentum of the scattered electron defines the momentum transferred to the target:

$$\boldsymbol{K} = \boldsymbol{p}_0 - \boldsymbol{p}_a. \tag{4}$$

Under the conditions where the ejected electron is in a direction close to that of the momentum transfer direction ($+K$), all momentum transferred to the target is absorbed by the outgoing electron. This minimizes the recoil momentum magnitude, and the collisions are said to be binary. Similarly, when the electron is directed in the direction opposite to that of the momentum transfer ($-K$), the recoil momentum of the residual ion is at its maximum, and the collisions are said to be recoil in nature.

The full details of our experimental apparatus and measurement procedure have been described previously,[13,19] so only a brief summary is repeated again here. An electron beam of fixed energy, $E_0 = 250$ eV, is generated through the thermionic emission of a tungsten filament. The emitted electrons are then accelerated, collimated, and focused into the interaction region by a 5-element cylindrical lens stack. The energy resolution of the incident electron beam was of the order of ~0.5 eV (FWHM). The electrons now interact with a pure beam of the target molecules (either THP or 1,4-dioxane) introduced through a capillary. Here, high purity samples were degassed by repeated freeze-pump-thaw cycles prior to being introduced into the system. During the measurements, the vacuum chamber and sample gas lines were heated to ~40 °C in order to minimize any absorption onto their surfaces. Scattered (fast) and ejected (slow) electrons, produced in ionizing collisions with the target beam, were detected in separate analyzers, mounted on independently rotatable turntables. Each analyzer consisted of a 5-element electrostatic lens, hemispherical energy selector, and channel electron multiplier. Using standard coincidence timing techniques, the arrival times of the electrons detected in each analyzer were used to determine if the electrons originated from the same ionization event.

For each cyclic ether, we measured its binding energy spectrum (BES, see later). These spectra are obtained at $E_0 = 250$ eV and $E_b = 20$ eV, while the scattered and ejected electron angles are fixed at $\theta_a = -10^\circ$ and $\theta_b = 75^\circ$, respectively. The BES for each target is obtained by measuring the number of true coincident events, as the scattered electron energy is repeatedly scanned over a range of detection energies. Here, the kinematics for the binding energy spectra measurements are selected to approximate bound Bethe ridge kinematics, where $|\boldsymbol{K}| \approx |\boldsymbol{p}_b|$, and we note that the typical coincidence binding energy resolution of the apparatus is 1.1 eV (FWHM) as determined from measurements of the Helium 1s binding energy peak. The kinematical conditions for the BES measurements were chosen to facilitate comparisons with photoelectron spectroscopy and electron momentum spectroscopy measurements by minimizing the influence of any scattering dynamics.

In the present work, TDCS measurements for a particular transition are obtained by fixing the scattered electron analyzer at $\theta_a = -5^\circ$ and by rotating the ejected electron analyzer in the scattering plane. In this way, we obtain angular distributions for the slow ejected electron. Here we again note that the incident electron and ejected electron energies are $E_0 = 250$ eV and $E_b = 20$ eV, respectively. The selected kinematics for our TDCS study now correspond to those below the bound Bethe-Ridge, and match those employed in our earlier study on THF.[15] Specifically, the magnitude of the momentum transfer, $|\boldsymbol{K}| = 0.45$ a.u., is much less than the momentum of the ejected electron, $|\boldsymbol{p}_b| = 1.21$ a.u. As such, a substantial linear momentum contribution to the outgoing electrons must arise from the internal momentum of the particles within the target. Under these conditions, below the bound Bethe-Ridge condition, the magnitude of the momentum transfer and the ejected electron's momentum are comparable to the momentum of the electrons bound to the target. Indeed, this kinematical condition has been most interesting in terms of our earlier dynamical (e,2e) studies on large biomolecules.[8–14]

III. THEORETICAL DETAILS

The present experimental data are compared to theoretical calculations obtained within a M3DW (molecular 3-body distorted wave) framework.[20–22] These calculations have been described elsewhere, so only a brief description is repeated here. The TDCS for the M3DW is given by

$$\frac{d\sigma}{d\Omega_a d\Omega_b dE_b} = \frac{1}{(2\pi)^5}\frac{k_a k_b}{k_i}\left(|T_{dir}|^2 + |T_{exc}|^2 + |T_{dir} - T_{exc}|^2\right), \quad (5)$$

where $\vec{k}_i$, $\vec{k}_a$, and $\vec{k}_b$ are the wave vectors for the initial, scattered, and ejected electrons, respectively, T_{dir} is the direct scattering amplitude, and T_{exc} is the exchange amplitude. The direct scattering amplitude is given by

$$T_{dir} = \left\langle \chi_a^-(\vec{k}_a, \mathbf{r}_1)\chi_b^-(\vec{k}_b, \mathbf{r}_2)C_{scat-eject}\left(r_{12}^{ave}\right) \times \left|V - U_i\right|\phi_{DY}^{OA}(\mathbf{r}_2)\chi_i^+(\vec{k}_i, \mathbf{r}_1)\right\rangle. \quad (6)$$

Here r_1 and r_2 are the coordinates of the incident and the bound electrons, χ_i, χ_a, and χ_b are the distorted waves for the incident, scattered, and ejected electrons, respectively, and $\phi_{DY}^{OA}(r_2)$ is the initial bound-state Dyson molecular orbital averaged over all orientations. Under the frozen orbital approximation, the Dyson orbital can be approximated using the initial bound Kohn-Sham orbital. The molecular wave functions were calculated using density functional theory (DFT) along with the standard hybrid B3LYP[23] functional by means of the ADF 2007 (Amsterdam Density Functional) program[24] with the TZ2P (triple-zeta with two polarization functions) Slater type basis sets. The factor $C_{scat-eject}(r_{12}^{ave})$ is the Ward-Macek average Coulomb-distortion factor between the two final state electrons,[25] V is the initial state interaction potential between the incident electron and the neutral molecule, and U_i is a spherically symmetric distorting potential which is used to calculate the initial-state distorted wave for the incident electron $\chi_i^+(\vec{k}_i, \mathbf{r}_1)$. For the exchange amplitude T_{exc}, particles 1 and 2 are interchanged in Eq. (6).

The Schrödinger equation for the incoming electron wave-function is given by

$$\left(T + U_i - \frac{k_i^2}{2}\right)\chi_i^+(\vec{k_i}, r) = 0, \quad (7)$$

where T is the kinetic energy operator and the "+" superscript on $\chi_i^+(\vec{k}_i, \mathbf{r})$ indicates outgoing wave boundary conditions. The initial state distorting potential contains three components $U_i = U_s + U_E + U_{CP}$, where U_s contains the nuclear contribution plus a spherically symmetric approximation for the interaction between the projectile electron and the target electrons, which is obtained from the quantum mechanical charge density of the target. The charge density is obtained by summing 2 $|\phi_{DY}|^2$ over all occupied orbitals (the 2 is for double occupancy and the original non-averaged Dyson orbital is used). The nuclear contribution to U_s is the interaction between the projectile electron and all the nuclei of the respective molecular target averaged over all orientations. Averaging the nuclei over all orientations is equivalent to putting the nuclear charge on a thin spherical shell whose radius is the distance of the nuclei from the center of mass (CM).

For THP, there are no nuclei located at the CM. The closest nuclei to the CM are the 2 carbon nuclei at 2.699 a_0. Consequently, the first nuclear sphere is constructed with a summed charge of 12 with a radius of 2.699 a_0. The next sphere describes the oxygen nucleus with charge 8 at 2.700 a_0. The third sphere is constructed for another two carbon nuclei with a total charge of 12 at a radius of 2.753 a_0, while the fourth sphere contains one carbon nucleus with a charge of 6 at a radius of 2.774 a_0. The fifth sphere has two hydrogen nuclei with a total charge of 2 at a radius of 3.728 a_0, while the sixth sphere describes one hydrogen nucleus with a charge of 1 at 3.823 a_0. The next 6 hydrogen nuclei are described by 3 spheres of charge 2 with radii of 3.827, 4.601, and 4.645 a_0, respectively, and the last sphere has 1 hydrogen nucleus with charge 1 at 4.681 a_0.

For 1,4—dioxane, also there are no nuclei found at the CM. The first nuclear sphere has 4 carbon nuclei with a total charge of 24 at a radius of 2.639 a_0. The next sphere has 2 oxygen nuclei with charge 16 at 2.668 a_0, while the 8 hydrogen nuclei are described by 2 spheres of charge 4 with radii of 3.707 and 4.521 a_0, respectively. Note that we present the radii to three decimal places to distinguish the closely spaced nuclear spheres, not because we necessarily believe that we have this level of numerical accuracy in our calculations. Note that the corresponding details of our calculations on THF can be found elsewhere.[15]

U_E is the exchange potential of Furness-McCarthy (corrected for sign errors),[26] which approximates the effect of the continuum electron exchanging with the passive bound electrons in the molecule, and U_{CP} is the correlation-polarization potential of Perdew and Zunger[27] (see also Padial and Norcross[28]).

In Eq. (6), the final state for the system is approximated as a product of distorted waves for the two continuum electrons (χ_a^-, χ_b^-) times the Ward-Macek average

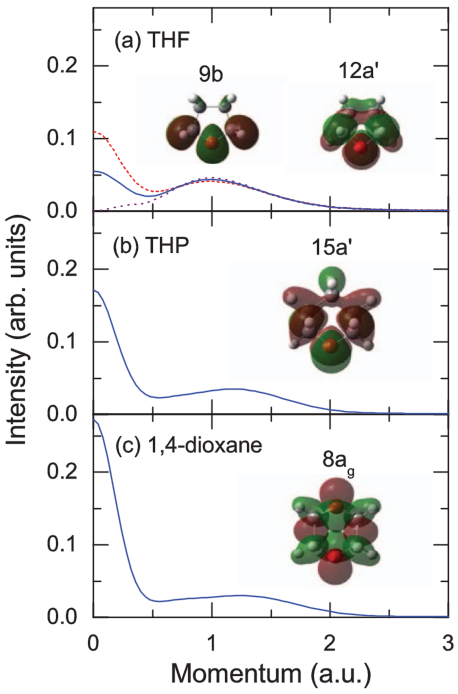

FIG. 2. Electron momentum profile and spatial representation of the HOMO for each cyclic ether. (a) 9b (· · ·), 12a′ (– –), and the conformational average of the 9b + 12a′ (—) orbitals of THF; (b) 15a′ orbital of THP; (c) $8a_g$ orbital of 1,4-dioxane. See text for further details.

Coulomb-distortion factor $C_{scat-eject}$. The final state distorted waves are calculated the same as the initial state except that the final state charge density is used to calculate U_s. The final state charge density is obtained the same as the initial state except that unity occupancy is used for the active electron orbital. Additional details can be found in Madison and Al-Hagan.[29]

To assist in the interpretation of the scattering phenomena, theoretical calculations to optimize the geometries and calculate molecular properties have been performed at the B3LYP/aug-cc-pVDZ level using GAUSSIAN 09.[30] These calculations have been utilized to generate electron momentum profiles for each target,[31] with the results being given in Fig. 2.

IV. STRUCTURE AND SPECTROSCOPY OF CYCLIC ETHERS

The structures of the cyclic ethers have attracted considerable interest.[32–35] On the one hand, THF has a relatively flat 5-member ring that possesses puckering out of the planar configuration, with the flatness of this ring structure producing a number of conformations that lie close in energy. Further, low potential energy barriers for pseudo-rotation between its conformations enable essentially free rotation between minima.[32,33] As such, THF exists in conformers with either C_2 or C_s symmetry found along the pseudorotation coordinate.[32,33] On the other hand, it has been well established that both THP and 1,4-dioxane exist in their lowest energy chair conformations.[34,35] These, respectively, have C_s and C_{2h} symmetries. In the interest of making fruitful comparisons regarding the behavior of these three cyclic ethers, we consider THF through an average over the C_2 to C_s conformations; with experimental results having revealed that both conformations exist in near equal proportions at room-like temperatures.[32,33] As our experiment is performed under room-like temperature conditions, this is a reasonable approximation given the complexity of the calculations. The full details of this averaging approach have been described elsewhere.[15]

Information regarding the ionization of the cyclic ethers has been obtained by ultraviolet photoelectron spectroscopy (PES),[36–38] Penning ionization electron spectroscopy (PIES),[36] and electron momentum spectroscopy.[33,39] In all the species under consideration, the HOMO is well separated from the other orbitals. Here the HOMOs are 9b + 12a′, 15a′, and $8a_g$ for THF, THP, and 1,4-dioxane, respectively. The calculated electron momentum profiles and spatial representation for the HOMO of each species are presented in Fig. 2. Each of these orbitals is dominated by the out-of-plane lone electron pair from the oxygen atom(s). Here, the structure of the target allows for varying degrees of interaction between the lone-electron pair and the carbon ring structure, with the non-bonding lone-electron pair interaction with the carbon frame increasing, as the structure changes in going from the relatively flat THF molecule to the chair conformation of THP. These interactions are further enhanced in 1,4-dioxane where there are also through-bond interactions that couple the lone-electron pair contributions from each of the oxygen atoms found in the ring. Note that this through-bond interaction energetically splits the molecular orbitals corresponding to the symmetric/asymmetric lone electron pair contributions.

The coupling of the lone-electron pair contributions to the carbon frame is particularly evident from the calculated electron momentum distributions presented in Fig. 2. Note that our calculated electron momentum profiles for THF and 1,4-dioxane are in reasonable qualitative agreement with measured electron momentum profiles from independent electron momentum spectroscopy experiments.[33,39,40] To our knowledge, there are no other theoretical or experimental data for the electron momentum profile of the HOMO of THP with which we can compare our calculation. Here we see that the electron momentum profiles for each species have two distinct features. Namely, there is the oxygen lone-electron 2p contribution that gives the local maxima at about 1.0–1.3 a.u. and the σ-contribution from the carbon frame at momentum $|\boldsymbol{p}| \sim 0$ a.u. In Fig. 2 we also see discernible trends in the electron momentum profiles, with the σ-contribution increasing from THF to THP and then to 1,4-dioxane, as the lone-electron pair(s) have larger interactions with the carbon frame. Note that the delocalization of the lone-electron pair through the carbon frame reduces the overall magnitude of the 2p oxygen contribution and shifts its peak to a higher momentum value. These peak values have intensities of 0.044, 0.035, and 0.030 and are located at 1.00, 1.16, and 1.24 a.u. for THF, THP, and 1,4,-dioxane, respectively. In 1,4-dioxane, this redistribution of intensity in the electron momentum profile is also expected to be influenced by the interference effects of having O(2p) contributions located on separated atoms, the so-called bond-oscillation phenomenon.[41]

While the structural changes across the series of cyclic ethers significantly affect the momentum distributions, these structural variations may have a minimal bearing on the scattering dynamics in the ionization of the HOMO for these species. Here the localized geometric perturbations surrounding the oxygen atom, in expanding the ring structure to accommodate the additional C atom in going from THF to THP, appear to be negligible. Specifically, the two closest C-atoms to the primary oxygen ionization site have bond distances of 1.43 Å, while making COC angles of ∼111°–112° for both THF (C_2) and THP. Note that for the THF (C_s) conformer, it has the same bond distances with a slightly smaller COC angle of 106°. Further, the CO bond distances and COC angles are also 1.43 Å and 111°, respectively, for 1,4-dioxane. We note that recent TDCS calculations on methane have revealed that a delocalization of the nuclear charge reduces the electron-nuclei post-collision interaction.[42] Bearing this in mind, perhaps of most importance in understanding ionization scattering dynamics is the proximity of the surrounding nuclei to the primary ionization site. We will examine this notion again later.

V. RESULTS AND DISCUSSION

In Fig. 3, the binding energy spectrum for each of the cyclic ethers is presented. Recall that all of these BES have been obtained under conditions where the incident electron is 250 eV, the scattered electron is detected at $\theta_a = -10°$, and the ejected electron is detected at $\theta_b = 75°$ with an energy of 20 eV. For each species, we note reasonable agreement regarding the location of features in the binding energy spectra with those previously observed in the PES and PIES experiments.[36,38] Each binding energy spectrum has been deconvolved using Gaussian functions whose widths represent the combination of the coincidence energy resolution from the experimental apparatus and the line widths of the ionization transitions, as estimated from the respective photoelectron spectra. This deconvolution procedure suggests that the HOMO of THP may be completely resolved from the other molecular orbitals. For THF (conformer independent) and 1,4-dioxane, while PES reveals that the HOMOs are well separated from the next highest occupied molecular orbitals (NHOMO), the limited energy resolution of our spectrometer suggests that the HOMOs may not be completely resolved from the NHOMOs in our measurements for these species. However, the NHOMO contribution to the HOMO peak in the BES would still be very small in these cases.

Figures 4(a)–4(c) show the experimental and theoretical TDCS results for the electron-impact ionization of the HOMOs of THF, THP, and 1,4-dioxane. For each cyclic ether, the cross sections have been measured with the incident electron having an energy of 250 eV and the scattered electron being detected at $\theta_a = -5°$. Once again the ejected electron is detected with an energy of 20 eV. Note also that our experimental measurements are relative, and to place them on the absolute scale they have been independently normalized to the M3DW theory in each case at $\theta_b = 65°$. While we note that experimental techniques exist for placing the (e,2e) measurements on an absolute scale,[43] such techniques are not possible here owing to the complexity of the ionization spectra for such large molecules. We further note that the quite large statistical uncertainties in our TDCS in Fig. 4 arise from the difficulties in performing coincident measurements under the present kinematical conditions.

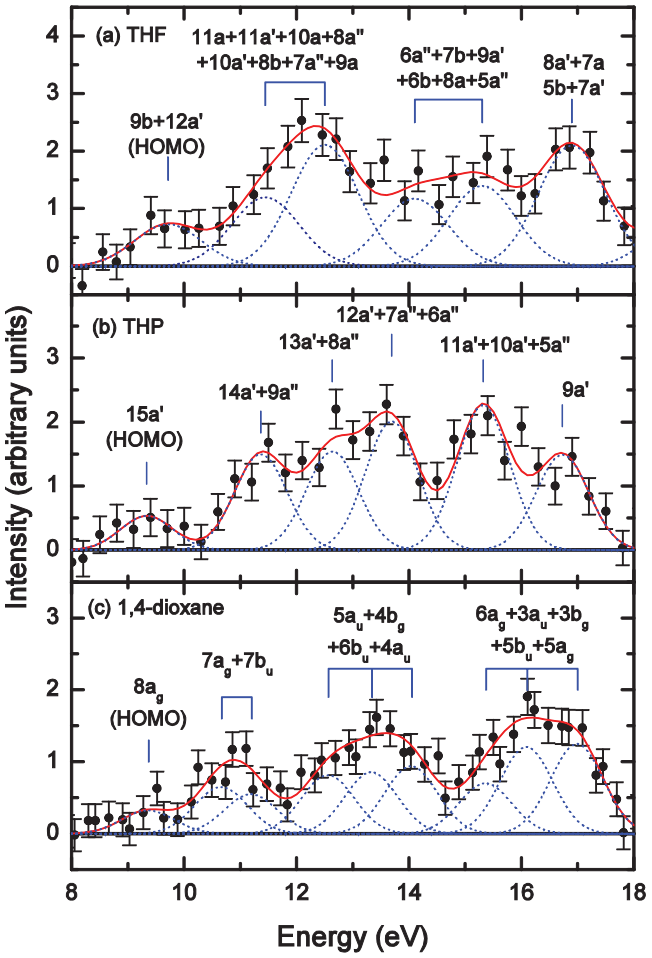

FIG. 3. Measured binding energy spectra (●) for (a) THF, (b) THP, and (c) 1,4-dioxane. Also shown are the spectral deconvolutions of the measured spectra into contributions from each orbital feature (– –) and their sum (—). See text for further details.

Considering Fig. 4, it is immediately apparent that the experimental binary peak for each species is particularly broad. Comparing these experimental results with those calculated, we observe that the width of the binary feature in each species is largely underestimated by the M3DW calculations. A possible exception to this is for 1,4-dioxane, where the M3DW calculation gave a broader peak than that calculated for either THF or THP. Although, even in this case, the M3DW cross section decreases more rapidly in magnitude than the experimental data at the larger ejected electron scattering angles ($\theta_b = 110°$–$120°$) in the binary region. The M3DW calculations of the cyclic ethers in this binary region are also particularly interesting, and those details are now discussed in turn.

First, the magnitudes of the cross sections for THF, THP, and 1,4-dioxane in the binary region are comparable. This may be somewhat expected as the HOMOs for the cyclic ethers are quite similar in their nature. Second, the maximum binary cross section intensity is calculated to be at 60°,

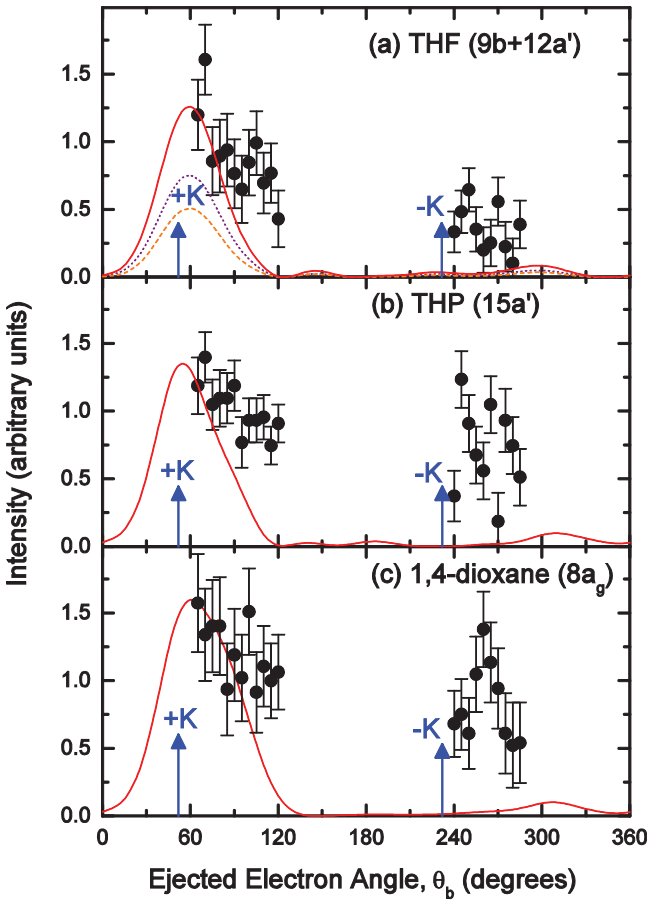

FIG. 4. Triple differential cross sections for the electron-impact ionization of the HOMOs of (a) THF (conformational average of the 9b + 12a′), (b) THP (15a′), and (c) 1,4-dioxane ($8a_g$) with E_0 = 250 eV and E_b = 20 eV. Measured experimental data (●). The M3DW calculation results (—) are also presented for each orbital or conformational average of contributing orbitals. Additionally shown are the TDCS contributions from the 9b (– –) and 12a′ (· · · · ·) orbitals of THF, after being weighted by their respective conformer populations. See text for further details.

55°, and 61° for THF, THP, and 1,4-dioxane, respectively. Here we note that the momentum transfer direction, under these kinematical conditions, for each of these cyclic ethers is 52°. The M3DW calculation gives larger shifts away from the momentum transfer direction for THF and 1,4-dioxane than that calculated for THP. Unfortunately, the broad nature and rather large statistical uncertainty, on the experimental data for the binary feature, does not allow us to make a quantitative assessment of any possible experimental shift in the binary peak.

Shifting our discussion to the recoil region, prominent recoil peaks are observed in the experimental data for each species. In this case, we observe in Fig. 4 that the strength of these recoil features, relative to that observed for the binary features, changes between the 5- and 6-member rings. For THF, the recoil peak is about a third of the intensity of the binary peak, while it is about two-thirds of the intensity of the binary peak for both THP and 1,4-dioxane. Interestingly, the experimental recoil data reveal quite broad flat features for both THF and THP, when the errors on the data are allowed for, while there is evidence of a quite prominent peak centered at $\theta_b = 260°$ for 1,4-dioxane. While significant experimental intensity is observed in the recoil region for each of the cyclic ethers, the M3DW model greatly underestimates the recoil feature intensity for each species. The absence of any important theoretical recoil peak contribution has also been observed in our earlier studies on large biomolecules.[9,10,15] This is attributed to weak electron-nuclear scattering arising from the need to spread the nuclear charge in the calculation over large spherical shells, in order to perform the spherical averaging over the random orientation of the molecule. The key to unlocking this information may involve considering the localized ionization of the lone-electron pair on an oxygen atom, however, such calculations are limited by the complexity in performing scattering computations on open-shell targets.

The trend in the measured binary to recoil ratios across the series of cyclic ethers is also quite interesting. Previously Xu *et al.*[44] have suggested that the origins of the observed binary-to-recoil ratio may be related to the electron momentum profile of the ionized molecular orbital. In earlier studies on THF,[12–15] the behavior of the binary to recoil ratios with respect to the variations in kinematical conditions could be qualitatively explained by relating the kinematical conditions to the ionized orbitals electron momentum profile. However, comparisons between the cross sections of THF and THFA[15] also revealed that the target molecular structure must play a role in the observed binary-to-recoil ratio. The cyclic ethers thus present an opportunity to discover the extent by which electron momentum profiles may influence the scattering dynamics. In the present work, the geometric perturbations in expanding the 5-member ring structure to accommodate the additional C-atom are negligible in going from THF to THP, such that any contribution arising from electron-nuclei scattering may be similar if the scattering dynamics are dominated by the nuclei closest to the ionization site. We now evaluate if the electron momentum profile can provide any clues for explaining the observed binary-recoil ratios in this series of structurally related cyclic ethers.

To assist in this discussion, the electron momentum profiles of Fig. 2 have now been plotted together in Fig. 5. Under the present kinematics below the bound Bethe-ridge condition, where substantial linear momentum contributions must arise from the internal momentum of the target particles, the range in magnitude of the recoil momentum values covered by the experiment in going from the binary to recoil region is $|\boldsymbol{q}| = 0.77$–1.66 a.u. Note that under such low-incident electron energy and low momentum transfer collisions, there is no guarantee that the recoil momentum is equal and opposite to the momentum of the bound electron at the time of ionization, as in electron momentum spectroscopy experiments,[45] however it may still provide insight into the observed physical behavior. Considering Fig. 5 in the momentum range 0.77–1.66 a.u., the electron momentum profile for the HOMO of THF starts at a higher intensity and decreases rather more rapidly than that for the HOMO of either THP or 1,4-dioxane. This observation may thus explain why the recoil peak intensity, relative to that observed for the binary, is lower for THF when compared to THP and 1,4-dioxane. Note also that the similar electron momentum profiles in this recoil momentum range for THP and 1,4-dioxane may also explain the similar binary to recoil peak intensities observed for those species.

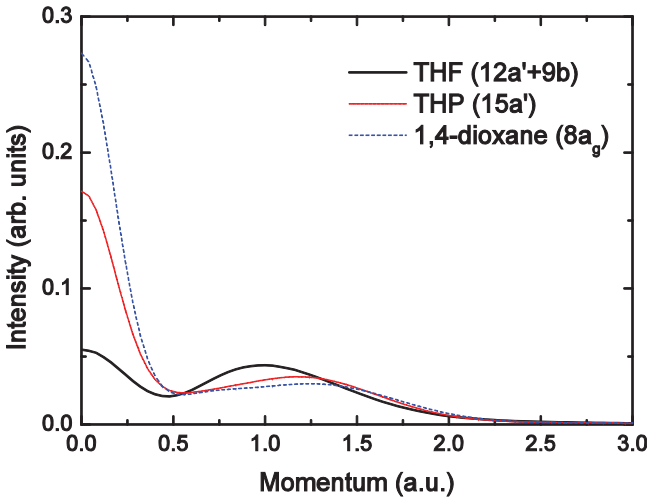

FIG. 5. Electron momentum profiles for the 9b + 12a′ orbitals of THF (—), the 15a′ orbital of THP (· · ·), and the $8a_g$ orbital of 1,4-dioxane (– –), now plotted on the one graph. See text for further details.

With the clues for the observed scattering behavior between THF and THP possibly being qualitatively described by their respective momentum distributions, it appears as though 5- and 6-member rings exert similar effects on the scattering dynamics. This result may be somewhat expected, as the geometric perturbations in expanding the ring structure to accommodate the additional C-atom may be negligible here. It is interesting to note that this behavior is markedly different from an earlier comparison between THF and THFA, where the addition of the exocyclic group appeared to perturb the scattering dynamics despite the electron momentum profiles of the two targets being similar. All of these observations initially suggest that we may be able to separate contributions from the orbital behavior and the scattering dynamics to the measured TDCS. This in particular alludes to the possibility of identifying key structural moieties that can be utilized for the purpose of modeling the scattering dynamics of the ionization process in combination with quantum chemical calculations.

VI. CONCLUSION

We have presented results from the first dynamical study of the electron-impact ionization of tetrahydropyran and 1,4-dioxane. Here the measured binding energies for each species were found to be in good agreement with earlier photoelectron spectroscopic measurements. The chosen kinematical conditions enabled a comparison with our earlier measurements on tetrahydrofuran in order to study the dynamics of the ionization process over a series of structurally related cyclic ethers under kinematics that fall below the bound Bethe ridge conditions. Across this series of cyclic ethers, the binary peak structures were seen to be quite broad with their widths generally being underestimated by our theoretical calculations. For each of the cyclic ethers, significant recoil peak intensity was observed and this was also largely underestimated by the present theoretical calculations. Our calculated electron momentum profiles suggest that they may yet provide key information into explaining the observed binary-recoil ratios in this kinematic regime. The present results also hint at the possibility for separating the orbital and structural contributions to the scattering phenomena under dynamical (e,2e) conditions. This would represent an important step in improving quantitative models for ionization phenomena in larger complex systems.

ACKNOWLEDGMENTS

This research was supported by the Australian Research Council (ARC) Centre of Excellence for Antimatter-Matter Studies, by the US National Science Foundation under Grant No. PHY-1068237 (H.C. and D.H.M.), and by the National Natural Science Foundation of China under Grant No. 11174175 (C.G.N.). G.B.S. thanks the CAPES (Grant No. BEX 17756/12-0) and Flinders University for financial assistance during his stay in Australia. D.B.J. gratefully acknowledges support provided through an ARC Discovery Early Career Researcher Award.

[1]L. Campbell and M. J. Brunger, Plasma Sources Sci. Technol. **22**, 013002 (2013).
[2]L. Chiari, M. J. Brunger, and A. Zecca, in *Radiation Damage in Biomolecular Systems*, edited by G. Garcia Gomez-Tejedor and M. C. Fuss (Springer, London, UK, 2012), pp. 155–163.
[3]I. Baccarelli, I. Bald, F. A. Gianturco, E. Illenberger, and J. Kopyra, Phys. Rep. **508**, 1 (2011).
[4]S. M. Pimblott and J. A. LaVerne, Radiat. Phys. Chem. **76**, 1244 (2007).
[5]H. D. Flosadóttir, B. Ómarsson, I. Bald, and O. Ingólfsson, Eur. Phys. J. D **66**, 13 (2012).
[6]B. Boudaiffa, P. Cloutier, D. Hunting, M. A. Huels, and L. Sanche, Science **287**, 1658 (2000).
[7]X. Pan, P. Cloutier, D. Hunting, and L. Sanche, Phys. Rev. Lett. **90**, 208102 (2003).
[8]D. S. Milne-Brownlie, S. J. Cavanagh, B. Lohmann, C. Champion, P. A. Hervieux, and J. Hanssen, Phys. Rev. A **69**, 032701 (2004).
[9]S. M. Bellm, J. D. Builth-Williams, D. B. Jones, H. Chaluvadi, D. H. Madison, C. G. Ning, F. Wang, X. G. Ma, B. Lohmann, and M. J. Brunger, J. Chem. Phys. **136**, 244301 (2012).
[10]J. Builth-Williams, S. M. Bellm, D. B. Jones, H. Chaluvadi, D. Madison, C. G. Ning, B. Lohmann, and M. J. Brunger, J. Chem. Phys. **136**, 024304 (2012).
[11]C. J. Colyer, M. A. Stevenson, O. Al-Hagan, D. H. Madison, C. G. Ning, and B. Lohmann, J. Phys. B **42**, 235207 (2009).
[12]C. J. Colyer, M. A. Stevenson, and B. Lohmann, J. Phys.: Conf. Ser. **194**, 052022 (2009).
[13]C. J. Colyer, S. M. Bellm, B. Lohmann, G. F. Hanne, O. Al-Hagan, D. H. Madison, and C. G. Ning, J. Chem. Phys. **133**, 124302 (2010).
[14]C. J. Colyer, S. M. Bellm, G. F. Hanne, O. Al-Hagan, D. Madison, C. G. Ning, and B. Lohmann, J. Phys.: Conf. Ser. **288**, 012007 (2011).
[15]D. B. Jones, J. D. Builth-Williams, S. M. Bellm, L. Chiari, C. G. Ning, H. Chaluvadi, B. Lohmann, O. Ingolfsson, D. Madison, and M. J. Brunger, Chem. Phys. Lett. **572**, 32 (2013).
[16]C. Szmytkowski, A. Domaracka, P. Mozejko, and E. Ptasinska-Denga, J. Chem. Phys. **130**, 134316 (2009).
[17]C. Szmytkowski and E. Ptasińska-Denga, J. Phys. B **44**, 015203 (2011).
[18]A. Zecca, E. Trainotti, L. Chiari, M. H. Bettega, S. Sanchez, M. T. Varella, M. A. Lima, and M. J. Brunger, J. Chem. Phys. **136**, 124305 (2012).
[19]S. J. Cavanagh and B. Lohmann, J. Phys. B **32**, L261 (1999).
[20]J. Gao, D. H. Madison, and J. L. Peacher, J. Chem. Phys. **123**, 204314 (2005).
[21]J. Gao, D. H. Madison, and J. L. Peacher, J. Phys. B **39**, 1275 (2006).
[22]J. Gao, J. L. Peacher, and D. H. Madison, J. Chem. Phys. **123**, 204302 (2005).
[23]C. Lee, W. Yang, and R. G. Parr, Phys. Rev. B **37**, 785 (1988).
[24]C. F. Guerra, J. G. Snijders, G. te Velde, and E. J. Baerends, Theor. Chem. Acc. **99**, 391 (1998).

[25]S. J. Ward and J. H. Macek, Phys. Rev. A **49**, 1049 (1994).
[26]J. B. Furness and I. E. McCarthy, J. Phys. B **6**, 2280 (1973).
[27]J. P. Perdew and A. Zunger, Phys. Rev. B **23**, 5048 (1981).
[28]N. T. Padial and D. W. Norcross, Phys. Rev. A **29**, 1742 (1984).
[29]D. H. Madison and O. Al-Hagan, J. At. Mol. Opt. Phys. **2010**, 367180 (2010).
[30]M. J. Frisch, G. W. Trucks, H. B. Schlegel *et al.*, GAUSSIAN 09, Revision B.01, Gaussian Inc., Wallington, CT, 2010.
[31]J. P. D. Cook and C. E. Brion, Chem. Phys. **69**, 339 (1982).
[32]A. Giuliani, P. Limão-Vieira, D. Duflot, A. R. Milosavljevic, B. P. Marinkovic, S. V. Hoffmann, N. Mason, J. Delwiche, and M. J. Hubin-Franskin, Eur. Phys. J. D **51**, 97 (2009).
[33]C. G. Ning, Y. R. Huang, S. F. Zhang, J. K. Deng, K. Liu, Z. H. Luo, and F. Wang, J. Phys. Chem. A **112**, 11078 (2008).
[34]H. E. Breed, G. Gundersen, and R. Seip, Acta Chem. Scand., Ser. A **33**, 225 (1979).
[35]D. M. Chapman and R. E. Hester, J. Phys. Chem. A **101**, 3382 (1997).
[36]M. Yamauchi, H. Yamakado, and K. Ohno, J. Phys. Chem. A **101**, 6184 (1997).
[37]T. Kobayashi and S. Nagakura, Bull. Chem. Soc. Jpn. **46**, 1558 (1973).
[38]K. Kimura, S. Katsuwata, Y. Achiba, T. Yamazaki, and S. Iwata, *Handbook of HeI Photoelectron Spectra of Fundamental Organic Molecules* (Japan Scientific Societies Press, Tokyo, Japan, 1981).
[39]T. C. Yang, C. G. Ning, G. L. Su, J. K. Deng, S. F. Zhang, X. G. Ren, and Y. R. Huang, Chin. Phys. Lett. **23**, 1157 (2006).
[40]T. Yang, G. Su, C. Ning, J. Deng, F. Wang, S. Zhang, X. Ren, and Y. Huang, J. Phys. Chem. A **111**, 4927 (2007).
[41]N. Watanabe, X. Chen, and M. Takahashi, Phys. Rev. Lett. **108**, 173201 (2012).
[42]I. Tóth and L. Nagy, J. Phys. B **43**, 135204 (2010).
[43]L. R. Hargreaves, M. A. Stevenson, and B. Lohmann, Meas. Sci. Technol. **21**, 055112 (2010).
[44]S. Xu, X. Ma, S. Yan, and P. Zhang, J. Chem. Phys. **136**, 237101 (2012).
[45]E. Weigold and I. E. McCarthy, *Electron Momentum Spectroscopy* (Kluwer Academic/Plenum Publishers, New York, 1999).